

1 Creating movable interfaces by micro-powder injection moulding

2
3 U M Attia*, M Hauata¹, I Walton¹, D Annicchiarico¹ and J R Alcock¹

4 ¹ Manufacturing and Materials Department, Cranfield University, Wharley End, Cranfield, Bedfordshire,
5 MK43 0AL, UK.

6 * Corresponding author. Present address: Manufacturing Technology Centre Ltd., Ansty Business Park,
7 Coventry, CV7 9JU, UK. Tel.: +442476701742. E-mail address: usama.attia@the-mtc.org

9 Abstract

10 This paper presents a novel in-situ technique to produce articulated components with high-
11 precision, micro-scale movable interfaces by micro-powder injection moulding (μ PIM). The presented
12 process route is based on the use of micro-scale sacrificial layer between the movable subcomponents
13 which is eliminated during the debinding step, creating a dimensionally-controlled, micro-scale mobile
14 interface. The fabrication technique combines the advantages of micro-powder overmoulding, catalytic
15 debinding and sintering. The demonstrated example was a finger bone prosthesis joint consisting of two
16 sub-components with an interface between components of 200 μ m in size. The geometries of the sub-
17 components were designed such that they are inseparable throughout the process whilst allowing them to
18 move relative to each other after the debinding stage. The components produced showed the feasibility of
19 the process route to produce readily-assembled meso-, and potentially micro-, scale articulated systems.

20
21 **Keywords:** Micro-powder injection moulding, Metal injection moulding, Micro-cavities, Micro-joints,
22 Microfabrication, Three-dimensional

24 1. Introduction

25 Small-scale joints are becoming crucial to the development of the next generation of meso-scale
26 devices. Articulated systems with movable interfaces are particularly important for meso- and micro-scale
27 components. Examples include finger bone replacements, known as phalangeal prostheses, which have
28 component sizes in the order of few millimetres and tolerances in the order of hundreds of microns, such
29 as those tested by Field (2008) and Middleton et al. (2011). Another application for micro-scale

components with moving joints are ‘micro-engines’, which are micro-scale, power generation devices, currently under consideration as replacements for batteries in consumer portable devices. Typical micro-engines have component sizes in the order of millimetres and tolerances in the order of tens of microns, such as the examples demonstrated by Hassanin and Jiang (2010) and Zhu et al. (2010). ‘Micro-manipulators’ is another example of micro-scale devices with articulated components, which are used to remove, manipulate or deliver micro-scale elements, for example cells in medical applications, which have different sizes and tolerances in the order of few microns to tens of microns. Kim et al. (2008) have presented demonstrations of such systems.

In spite of the growing applications of metallic components with movable structures, current processing routes pose several constraints on the design and manufacturing routes of such complex structures. Such constraints result in considerable increase in manufacturing time and cost.

Whilst fabrication processes for the construction of multiple rigid bodies and their connecting joints - known as kinematic chains - are well characterized at the conventional (macro-) scale, at the micro-scale processes are still in their infancy. This is due to a number of challenges, the most significant of which are: a. limitations on the geometry of fabricable structures, b. material selection limitations, c. assembly challenges, d. powder-based fabrication challenges and e. mass manufacturability.

In terms of geometry limitations, joints possess usually one, or exceptionally two, degrees of translational or rotational freedom, a limitation imposed by the variants of ‘axial’ processes (normally lithography or cutting) used in their fabrication. This is evident in the examples available in the literature, such as movable, silicon-based micro-structures produced by Fan et al. (1988) for sensors and actuators, movable microfluidic elements demonstrated by Ling and Lian (2007) using SU-8 fabrication, silicon-based, micro-hinges produced by Pister et al. (1992) and movable micro-gears fabricated from SU-8 by Seidemann et al. (2002).

The second limitation imposed on meso- and micro-scale movable structures is materials selection. Such structures are severely restricted in terms of possible materials. As illustrated above, materials used for such applications are currently usually either silicon or SU8 (an epoxy-based photoresist). Such materials are notable for their poor wear resistance in moving parts, as illustrated by both Waits et al (2007) and Hergert et al. (2010) in two independent experiments about wear damages induced in micro-scale ball bearings produced by silicon fabrication techniques.

Assembling relatively small structures is another major challenge, because such assemblies are currently done by post-processing techniques and, therefore, require accurate alignment and tolerance checking. As mentioned above, currently, in-situ alignment has only been achieved with lithographic techniques using materials of limited mechanical performance, notably silicon and SU8. A number of such assembly techniques have been reviewed by Leong et al. (2010) for micro-scale components. For relatively-larger, meso-scale systems, post-processing assembly is usually implemented, such as a press-fit mechanism, as illustrated by Koch and Sandoz (1994) for metal finger joint prosthesis.

To overcome the material and geometrical limitations of silicon and SU8, some recent research has started to investigate the use of powder-based fabrication of micro-scale joints. Additive manufacturing, for example, has been investigated by Yang et al. (2011) for manufacturing conventionally-sized metal joints by laser selective melting. However, the process is comparatively slow and not optimized for micro-scale applications. On the micro-scale, recent work has attempted to produce micro-scale moving joints using powder-based ceramics. The idea was to co-sinter two components made of different materials in order to achieve the clearance required to facilitate motion by difference in volumetric shrinkage of the two materials. Demonstrations have been made by Pirotter et al. (2010a and 2010b) and Ruh et al. (2008 and 2010) using powder injection moulding. Such a procedure requires careful adjustment of process conditions to achieve the exact shrinkage in subcomponents, such that a movable clearance is achieved.

The challenge of mass manufacturability of assembled structures is associated with a number of obstacles. Firstly, post-processing assembly extends the time and cost of the process chain to ensure accurate alignment and movement, especially if the microfabrication process itself is relatively slow. Secondly, in case of in-situ assembly using silicon etching or similar techniques, the process is not mature enough for mass-fabrication.

This paper presents a technique using metal powders to produce moving components with dimensionally controlled micro-scale interfaces by μ PIM as a high-volume microfabrication process. A review of the μ PIM and its applications for micro-scale components is available in the literature (Attia and Alcock, 2011a). The following sections detail the proposed methodology through a demonstrator, and the discussion will assess the capability of the proposed technique to overcome the five challenges highlighted above.

2. Experimental

2.1 Methodology

Here we report on a strategy by which articulated architectures with micro-scale 3-D cavities can be fabricated using a lost-core approach. The authors have previously demonstrated the possibility of producing dimensionally controlled, enclosed micro-cavities by sequential powder over-moulding of metals (Attia and Alcock, 2012) and ceramics (Attia and Alcock, 2011b).

The hypothesis explored here was that a further development of such a methodology could be used to create “open” cavities/spaces between two or more components, such that the components could move relative to each other. Figure 1 presents a schematic illustration of the technique.

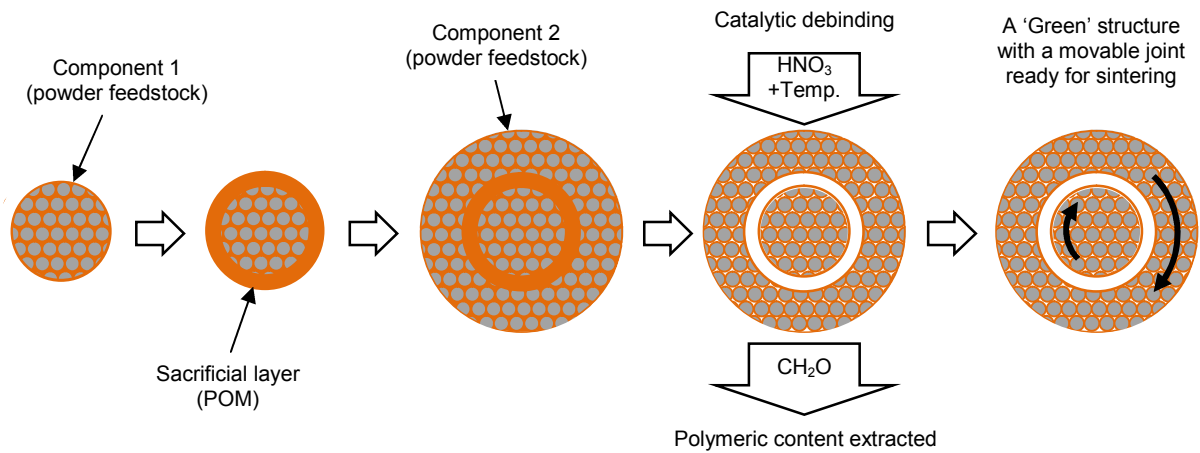


Fig. 1. A schematic illustration of catalytic debinding with a sacrificial core.

Briefly, one component is fabricated out of a metallic feedstock by μPIM . A micro-scale polymeric sacrificial layer is then overmoulded in the position relative to the first component at which a cavity is eventually required. The second component, made of powder feedstock, is overmoulded on top of the polymeric layer, ensuring, in the design and fabrication steps, that it has no contact points with the first component.

The resulting rigid structure is then catalytically debound, where nitric acid vapour is used to hydrolyse the POM of both the sacrificial layer and the components' binder into formaldehyde, which is extracted during the process. The resulting space allows for a relative motion between the two components, which are subsequently sintered for full densification.

The powder feedstock consists of the metallic powder, mixed with a catalytically debindable polymer, in this case polyoxymethylene (POM). The sacrificial layer is made of the same polymer so that both the polymeric content of the powder feedstock and the core could be simultaneously eliminated during catalytic debinding.

Stainless steel 316L was the material selected for this experiment for two main reasons. Firstly, stainless steel 316L is commercially available as a readily mixed feedstock consisting of powder particles with relatively small mean sizes (4-5 μm), which makes it suitable for micro-moulding applications. Using a commercial grade of feedstock makes it possible to assess the viability and consistency of the proposed process independent of factors related to mixing special medical grade powders.

The second reason for using 316L is that it is one of the most widely used materials for replicating conventional and micro-scale features by metal injection moulding (MIM). There is a considerable amount of previous work that looked into investigating different aspects of the powder injection moulding of 316L.

For example, with regard to mixing and characterising 316L feedstock, Liu et al. (2005) used 316L to assess the effects of powder loading and mixing conditions on feedstock homogeneity and shape retention of micro-moulded features. Abolhasani and Muhamad (2010) developed a new 316L feedstock for MIM based on starch as a binding material. Samanta et al. (2011) characterised the thermo-physical properties of an in-house mixture of a 316L feedstock for MIM. Kong et al. (2012) demonstrated a procedure to determine the optimal powder loadings for 316L stainless steel feedstock for micro-powder injection moulding.

With regard to process development, Loh et al. (2003) used 316L feedstock to replicate microstructure arrays with aspect ratios up to 2 using silicon inserts. Their work focused on the effect of process conditions on replication quality of micro-scale features.

Debinding 316L has also been investigated in a number of experiments. For example, Omar et al. (2003) demonstrated a two-stage rapid debinding technique combining solvent and thermal debinding of 316L feedstock. Li et al. (2003) compared the binder removal rate in vacuum and hydrogen environments during thermal debinding of 316L. The effect of thermal debinding of 316L feedstock on surface roughness of moulded components was also studied by Liu et al. (2007).

With regard to using 316L in variant MIM processes, Rota (2002) demonstrated the principle of sinter-bonding of two 316L components produced by micro-metal injection moulding. Nishiyabu et al. (2007) demonstrated a lost-core technique to produce microstructured 316L components by micro-injection moulding. In addition, Imgrund et al. (2008) co-injection moulded 316L and 17-4PH to produce magnetic-nonmagnetic bimetals by micro-MIM. 316L powder was also used by Manonukul et al. (2010) to demonstrate a technique to produce metal foam by metal injection moulding using a powder space holder.

With regard to properties of sintered 316L components, Castro et al. (2003) studied the mechanical properties and pitting corrosion behaviour of 316L. Tay et al. (2005) investigated the effect of sintering conditions on the surface roughness of microstructured components produced by injection moulding of 316L. Huang and Hsu (2009) compared the effect of three backbone polymers on the mechanical properties of 316L specimens produced by MIM, showing that HDPE performs best in terms of both the flow stability and the MIM compact quality. Rafi Raza et al. (2012) studied the effects of cooling rate on mechanical properties and corrosion resistance of vacuum sintered powder injection moulded 316L stainless steel. They showed that higher cooling rates improved mechanical properties and corrosion resistance compared to lower cooling rates.

Catalytic debinding was particularly selected for the process route presented in this paper, because it is a direct solid-gas transition process that takes place below the T_g of the polymer. The process, therefore, results in higher dimensional accuracy, tighter tolerances and better surface finish relative to other debinding techniques (German, 1998). Such characteristics make catalytic debinding an attractive process for applications requiring dimensional accuracy and tight tolerances. A recent market study has showed that 21% of the MIM industry currently relies on catalytic debinding (German and Atre, 2013)

Catalytic debinding of 316L has been investigated in several experiments. Examples include the work reported by Fu et al. (2004), where the use of uMIM to produce 316L microstructural arrays of high-aspect ratios was investigated in a process that involved catalytic debinding. The same group also studied the effect of moulding process parameters on the filling quality of the array microstructures (Fu et al., 2005a) and used catalytic debinding to produce microstructural arrays made of 316L with good shape retention (Fu et al., 2005b).

2.2 Experimental procedure

2.2.1 Structure design and operation

The application presented in the paper is a finger bone replacements, which has component sizes in the order of few millimetres and tolerances in the order of hundreds of micrometres. Similar prosthesis are usually fabricated as separate components and assembled by post processing as previously discussed in the introduction.

The structure selected for illustrating the process chain is for a finger-bone prosthesis, which was selected as a demonstrator for the proposed process for a number of reasons:

- i. The structure consists of moving components with micro-scale tolerances in the order of hundreds of microns.
- ii. The geometries of the subcomponents are three-dimensional in nature, with free-form surfaces within the joint itself, which makes them unsuitable for conventional 2½-D manufacturing processes.
- iii. The structure requires assembling the two-subcomponents, which is done as a post-processing step in state-of-the-art designs, and which this work attempts to do it in-situ (more details about the design of the assembly mechanism in the description of figure 2 below).
- iv. Such a component poses special material requirements in terms of mechanical properties and biocompatibility, which could be fulfilled with powder technology.

The process presented in Figure 1 was implemented to fabricate a readily assembled prosthesis consisting of a cylinder and socket structure. The cylinder and socket subcomponents will be referred to as “part 1” and “part 2”, respectively, throughout the text.

Figure 2 shows a CAD illustration of the structure with the main dimensions. The structure consists of two sub-components joined in a cylinder-and-socket format with a one-degree-of-freedom (DOF) mobility.

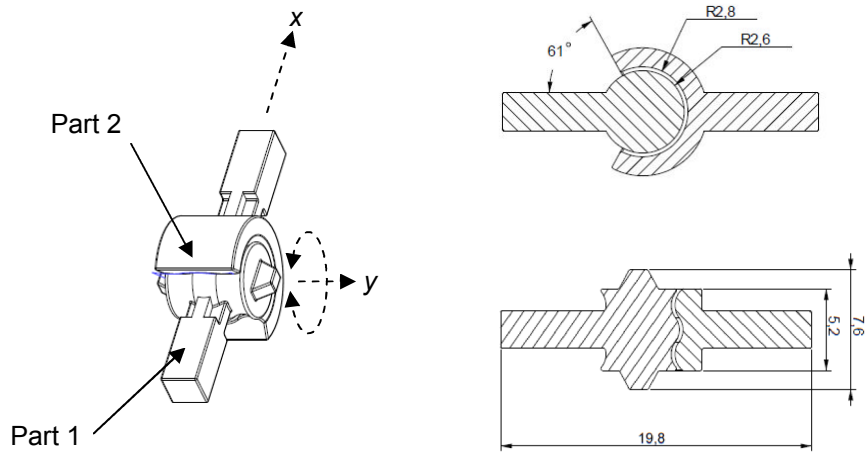


Fig. 2. A CAD illustration of the moving joint (all dimensions are in millimetres).

The in-situ assembly mechanism is achieved through the free-form design of the mating surfaces of the subcomponents that are designed such that they are inseparable throughout the manufacturing process. This design philosophy constrains the relative motions of parts 1 and 2 in all directions, except for the required 120-degree rotational movement around the y -axis. Part 1 is designed as a cylinder with a symmetrical curved surface. A similar curvature is introduced into the inside geometry of the socket of part 2, leaving a space of 200 μm between the mating surfaces of Parts 1 and 2, such that the two components are constrained in all translational and rotational directions except for rotation around the y -direction (figure 2).

Part 2 is designed such that the C-shape partially surrounds the cylinder of part 1 making them inseparable in the x -or z -directions. The C-shape of part 2 is designed to allow the required a rotation angle of 120° around the y -axis.

Both the cylinder and socket are attached to two “arms” that would be inserted into the bones during an operation to insert the prosthesis. In a finalized design, the two arms should have a particular design and structure to fulfil this purpose. In this particular case, they were designed as plain square-sectioned geometries for simplicity. The arms are connected to the cylinder and socket by four ribs each.

2.2.2 Fabrication methodology and procedure.

The mould used in this experiment was designed such that a replaceable steel insert carries the cavity that is filled with the feedstock during each moulding stage. This enables a quick replacement of

the insert without the need to replace the whole mould. Throughout this paper, an “insert” will refer to the replaceable part of the mould that carries the required cavity.

The fabrication methodology was planned following the sequential procedure shown in figure 1. Figure 3 (a to f) shows a schematic illustration of the fabrication sequence.

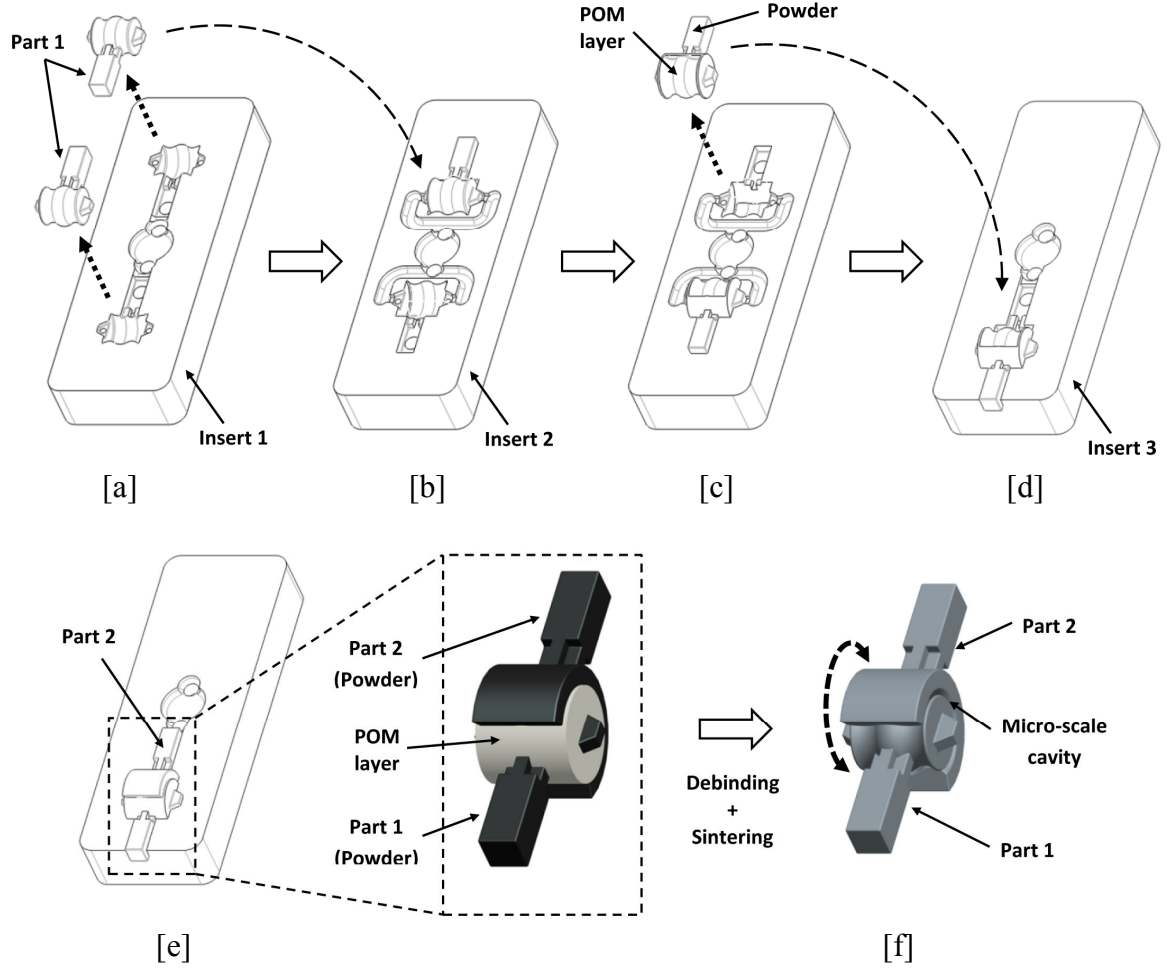


Fig. 3. A schematic diagram of the moulding process of a hybrid structure: (a) two pieces of Part 1 are moulded of 316L and ejected from insert 1. (b) Part 1 pieces are placed in the cavities of insert 2. (c) Part 1 pieces are overmoulded by 200-micron layers of POM and ejected. (d) One overmoulded structure is placed in the cavity of insert 3 ready for the second overmoulding step. (e) In the second overmoulding stage, Part 2 is moulded of 316L, resulting in a hybrid structure of Part 1, POM layer and Part 2. (f) After debinding and sintering, Part 2 is movable relative to Part 1.

- Step 1: Part 1 is moulded by μ PIM using a powder feedstock.
- Step 2: Part 1 is positioned inside another insert that is machined with extra cavity space for the polymer layer.

- Step 3: The sacrificial polymeric layer is micro-overmoulded around part 1 in the defined cavity space.
- Step 4: The resulting compound structure is positioned in a third insert that holds the cavity of part 2.
- Step 5: Part 2 is overmoulded by μ PIM using a powder feedstock.
- Step 6: The resulting compound structure is catalytically debound, resulting in the removal of the polymeric content, including the sacrificial layer.
- Step 7: The resulting structure is sintered for full densification.

2.2.3 Insert fabrication

The procedure shown in figure 3 illustrates that three micro-moulds are required to produce the ‘green’ compound structure. These moulds were fabricated as replaceable inserts in a single mould body. The six halves of the inserts were fabricated by micromilling.

The machined geometries were characterized by freeform surfaces and high-aspect ratio cavities. Such complex structures required special micro-cutting tools and special machining sequences, particularly during the finishing stage, to control the final micro-space between the moving components. Sintering shrinkage for the selected powder material is typically between 14% and 16%, so oversized mould cavities were designed and machined taking the final size of the structure into consideration.

Inserts were manufactured in hardened steel (Toolox® 33) using a KERN Evo micro-milling machine. A set of cutting micro-tools was used to cut and finish the inserts, where each cavity is machined with three roughing stages and one finishing stage. Table 1 summarizes the machining procedure for the three inserts.

Table 1. Micromilling procedure for the three inserts.

	Mould 1			Mould 2			Mould 3		
	Tool dia. (mm)	Rot. Speed (rpm)	Feed rate (mm/min)	Tool dia. (mm)	Rot. Speed (rpm)	Feed rate (mm/min)	Tool dia. (mm)	Rot. Speed (rpm)	Feed rate (mm/min)
Roughing	1	17600	530	1	17600	530	1	17600	530
Re-roughing 1	0.5	38000	480	0.5	38000	338	0.5	38000	369
Re-roughing 2	0.5	38000	404	0.5	38000	512	0.5	38000	500
Finishing	0.4	41000	420	0.4	41000	420	0.2	41000	26

2.2.4 Sequential micro-overmoulding by μ PIM

Powder micro-moulding was used to produce the green hybrid structure following the procedure above. The moulding conditions of both the powder feedstock and the polymer layer are shown in table 2.

Table 2. Moulding conditions for POM and powder/POM.

Material	Melt temperature [°C]	Mould temperature [°C]	Holding pressure [bar]	Injection velocity [mm/s]	Cooling time [s]
POM	190	100	300	250	10
Powder / POM	190	140	300	250	10

Polymer moulding and powder overmoulding were performed using a Battenfeld Microsystem 50 micro-moulding machine. The polymeric layer was moulded of POM (BASF Ultraform[®] W2320 003) with melt flow index of 25 to ensure better filling of micro-cavities; the powder feedstock was composed of a mixture of 316L stainless steel particles with average particle size (d_{50}) of 4 μ m and POM (BASF Catamold[®] 316LS).

2.2.5 Catalytic debinding and sintering

During debinding, the compound green structures were placed on a loose-powder bed of alumina for two reasons: Firstly, the powder was used to support the two arms of parts 1 and 2. This is because when the two parts become detached from each other after the removal of the polymer, the torque produced by the weight of the two arms might cause the corresponding parts to tilt against each other and touch at some point, which upon sintering could form a permanent joint. Secondly, the powder bed offers a “flexible” substrate that would not restrict the uniform shrinkage of the two parts due to, for example, friction. The loose powder would allow a simultaneous uniform volumetric shrinkage to take place in the two parts, including the gap in-between, without geometrical deformation.

Catalytic debinding took place following the BASF technique (Bloemacher and Weinand, 1997) at a dwell temperature of 110°C in high-concentration nitric acid (>98%) at an acid feed of approximately 30 ml/h. Debinding takes place following the so-called “shrinking core mechanism”, by which POM is eliminated layer-by-layer from the outside into the core. Nitrogen was used as a purging gas at a flow rate of approximately 500 l/h. The debinding cycle takes approximately 5 to 6 hours.

After debinding, the structure was composed of parts 1 and 2 in powder form between which there was a hollow space. At this stage, the two components were technically separate, although they

were fixed in place using the powder bed. The resulting ‘brown’ components were taken directly to the sintering oven while on the powder platform.

Sintering was conducted following the schedule shown in table 3, with hydrogen as the gaseous environment. The alumina powder bed facilitated the sintering process by holding the components in place and at the same time allowing them to shrink without bringing them to contact during sintering.

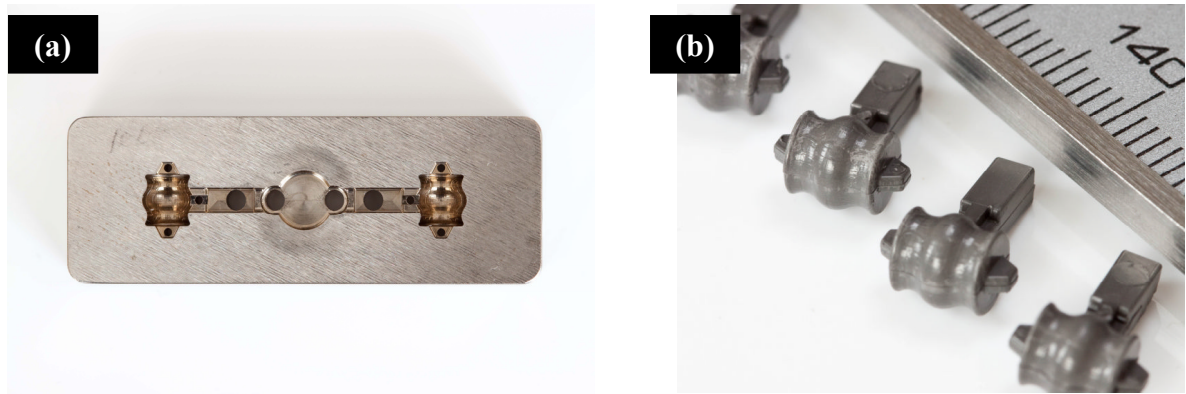
Table 3. Typical sintering schedule for Catamold 316L debound structures.

Stage	Schedule
1	From room temperature to 600°C at the rate of 3°C/min.
2	Hold at 600°C for 1 h.
3	From 600°C to 1250°C at the rate of 3°C/min.
4	Hold at 1250°C for 1 h.
5	From 1250°C to 600°C at the rate of 5°C/min.
6	Furnace cooling.

The density of the sintered components has been measured using the Archimedes principle, and hardness values have been measured by nanoindentation. Both values have been compared to the theoretical values supplied by the material manufacturer.

3. Results

Figure 4 shows the results of the micro-machining and micro-overmoulding procedure described earlier in section 2.2.2.



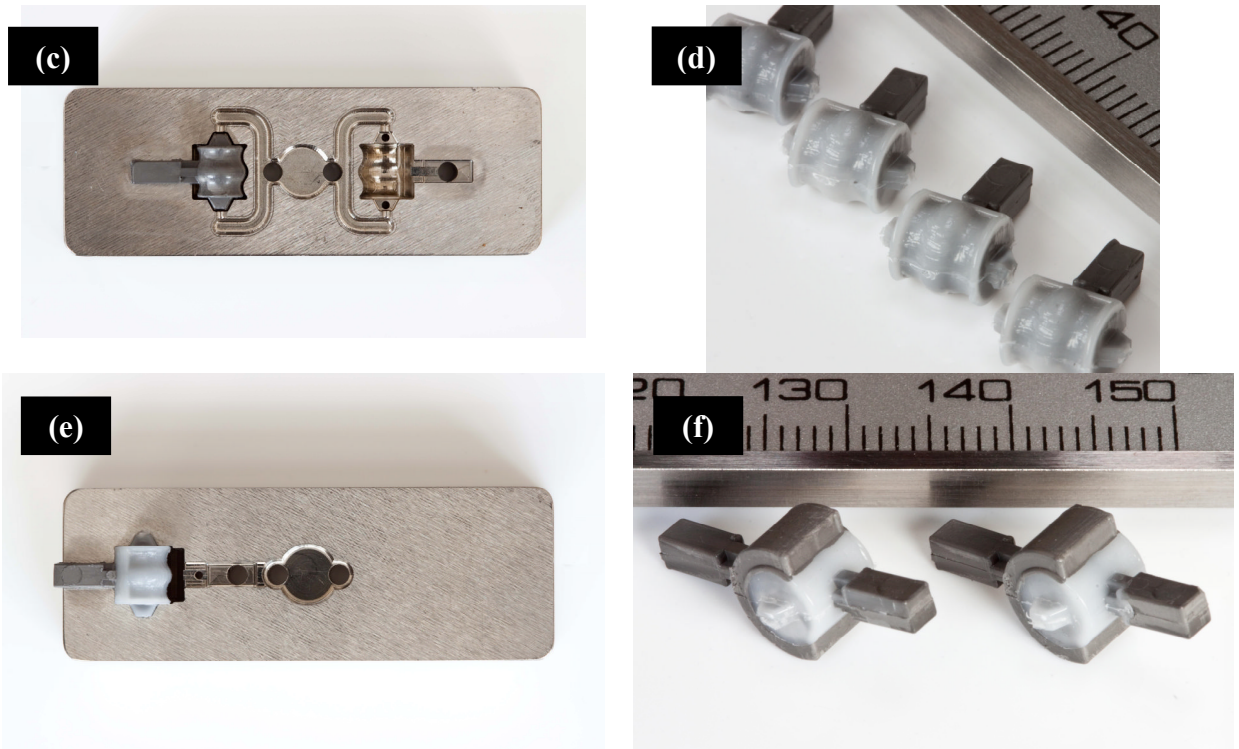


Fig. 4. (a) a twin-cavity insert for part 1 (b) part 1 samples replicated from 316LS feedstock (c) a twin-cavity insert for POM layer with part 1 sample placed in one cavity for illustration (d) part 1 samples micro-overmoulded with POM layers (e) an insert for component 2 with the overmoulded part 1 for illustration (f) samples of the complete hybrid green structure of parts 1 and 2 with the POM layer.

Figures 4a and 4b show the mould of part 1 and the replicated green component, respectively. The micro-moulding of the sacrificial POM layer is shown in figures 4c and 4d, where the former shows the mould in which part 1 was positioned, and the latter shows part 1 covered with the sacrificial POM layer where the moving space is eventually required. Figure 4c shows how the mould was designed with two registration cavities to secure the positioning of part 1 inside the mould whilst the POM layer is being overmoulded. The overmoulding of part 2 is shown in figures 4e and 4f, where the former shows the third, and final, mould cavity, and the latter shows the full compound hybrid structure.

Figure 5 shows a cross section in the hybrid green structure. The figure shows a symmetric layer of POM between parts 1 and 2 with variable thickness. Measurements indicate an average thickness of 246 μm at narrowest distance in the middle. The largest distances at the sides have average thicknesses of 367 μm .

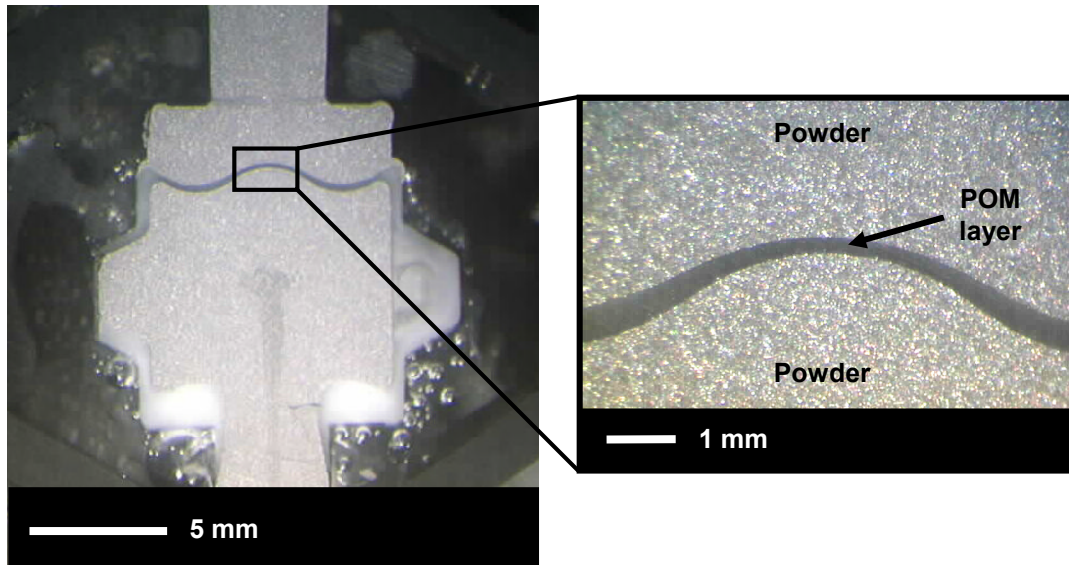


Fig. 5. A cross section in a green structure with an enlarged view of the micro-sacrificial layer.

Figure 6 shows a batch of “brown” structures after catalytic debinding positioned on the powder bed. The figure shows each structure consisting of two distinct components with a cavity in between with no visible traces of polymeric material.

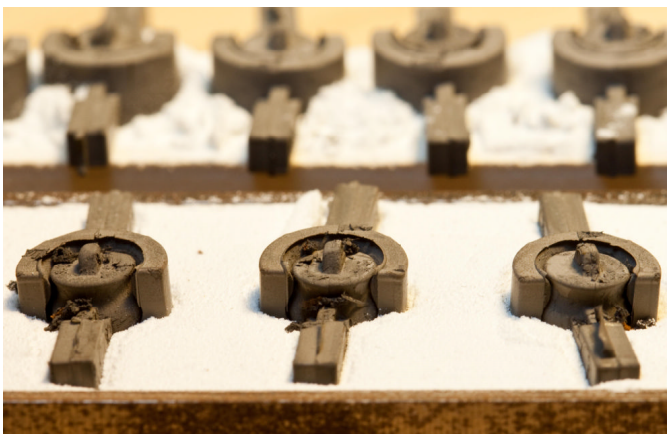


Fig. 6. Brown structures on a powder bed after catalytic debinding.

Figure 7 shows the final structures after sintering with a movable joint produced between the sub-components.



Fig. 7. Sintered structures with movable joints.

Figure 8 shows microscopy images of cross sections in the sintered components. Figure 8a is a cross section normal to the rotation axis, whilst figure 8b is a cross section parallel to the registration features. The images show the micro-cavity between the two subcomponents.

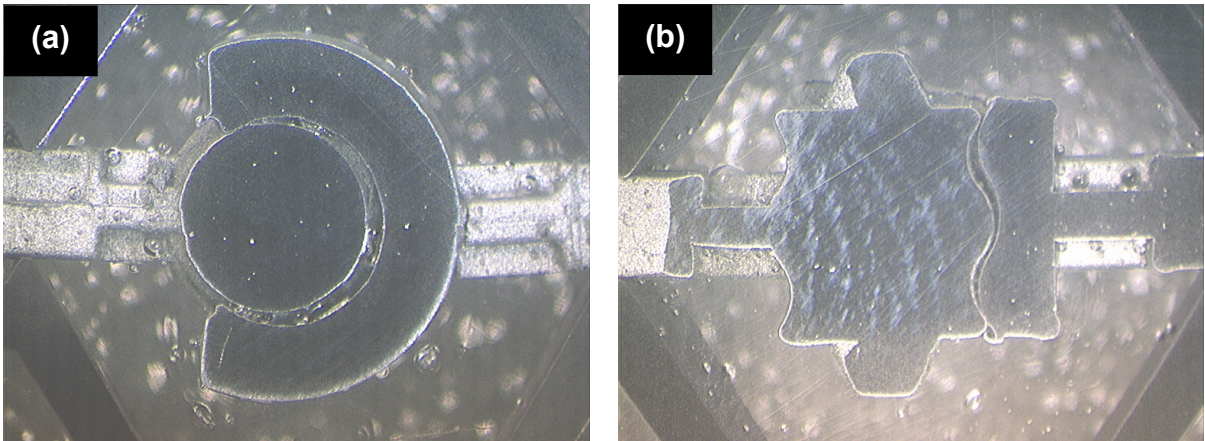


Fig. 8. Cross sections in the sintered structure (a) normal to the rotation axis and (b) parallel to the registration features.

Measurements were taken at different points close to the middle of the curved cavity and an average distance of approximately $218\text{ }\mu\text{m}$ was measured. The results illustrated in figures 7 and 8 show that the presented manufacturing technique is viable for producing micro-scale movable interfaces. The micro-overmoulding sequence in figure 4 shows that it is feasible to micro-mould dimensionally

controlled sacrificial geometries between powder-based components. The following discussion addresses how the proposed process chain has addresses the five challenges highlighted in section 1.

Table 4 shows the density measurements for six samples of the sintered components. The density is also presented as a percentage of the theoretical density specified by the material datasheet (7.9 g/cm^3).

Table 4. Density measurements of six sintered samples

No.	Density [g/cm^3]	% theoretical
1	6.577	83
2	6.533	83
3	6.670	84
4	6.548	83
5	6.716	85
6	6.651	84
Av.	6.616	83.7

Table 5 presents the results of Vickers hardness values obtained by nanoindentation measurements of five samples. The measurements were taken in two locations with 200-gram load: (a) on the circular section of part 1 and (b) on the arm section of part 2.

Table 5. Micro-hardness measurements of five samples in two locations.

No.	Part 1 hardness [HV]	Part 2 hardness [HV]
1	121	132
2	123	122
3	124	99
4	119	132
5	124	135
Av.	122.2	124

4. Discussion

In light of the results of section 3, this section evaluates how the proposed methodology addressed the processing challenges of meso- and micro-scale joints highlighted in the introduction.

With regard to the geometrical challenge, the results of figure 4 show that the process is viable in two aspects. Firstly, the micro-overmoulding procedure was performed for truly three-dimensional geometries with free-form surfaces, and the images of the moulded components in figure 4 (b, d and f) show good replication fidelity. Secondly, it was suspected that using the same polymer (POM) for both the powder matrix and the core might increase the likeliness of deformation at the interface due to the similar thermal properties. However, this was not observed during processing, and the cross section in

figure 5 shows a hybrid green component with good shape retention and clear boundaries between the powder shell and the polymer micro-layer.

With regard to the material variety challenge, the presented process is applicable to any powder-base mouldable feedstock. Commercially available feedstock covers a wide range of metals and ceramics with different mechanical, thermal and biomedical properties. In addition, powder feedstock with relatively small average particle sizes (in the order of few micrometres for metals and a few hundred nanometres for ceramics) is available, which enables the replication of meso- and micro-scale components. The presented process, therefore, offers a true shift from conventional materials associated with microfabrication such as silicon and SU8.

With regard to the assembly challenge, figures 5 and 6 show that the two parts are readily assembled and movable relative to each other. This was achieved in-situ by combining a design solution with a processing solution. The former was concerned with designing the internal geometries of both parts such that they are inseparable once a cavity is created between them. The latter solution was concerned with planning the processing steps such that alignment is readily achieved during the overmoulding stages by using registration marks and positioning constraints in the mould structure. This manufacturing strategy enables in-situ assembly, alignment and motion already after the debinding stage. The sintering stage was just to treat the components into the final density.

With regards to powder-based fabrication challenges, figure 6 of the debound components shows that the manufacturing principle is viable for producing sacrificial micro-cavities for powder-based moving joints. Unlike previous work reported in the literature that relied on controlling shrinkage rates to produce a movable interface, this approach overcomes this challenge by creating the interface through a micro-moulded sacrificial layer that precisely defines the final clearance between the moving components.

The images show that the POM micro-layer was totally consumed whilst the overall component retains its geometry. Other than a few defects inherited from the moulding process, such as the broken-gate remains or ejection-pin marks, the debinding process did not distort the geometrical integrity of the structure.

The cross sections of the sintered component illustrated in figure 8 show the cavity maintained in the structure. No visible signs of deterioration have been detected, and shape retention appears of high quality. Again no signs of particular problems related to cavity encapsulation were observed. The

measured cavity was approximately 218 μm , which corresponds to a linear shrinkage of approximately 11% from the 246- μm POM layer. This shrinkage is slightly lower than the 14% specified by the powder feedstock datasheet, which implies the need for better process control during sintering.

Density measurements reported in Table 4 show that the component density is about 84% of the theoretical density specified by the material manufacturer. This could be explained by the fact that sintering took place at 1250°C (maximum allowed by the equipment available), which is 100 degrees lower than the recommended 1360 °C sintering temperature recommended by the material supplier. The lower temperature was not sufficient to reach full densification. This also explains the lower value of shrinkage discussed earlier.

Hardness values reported in Table 5 shows that average values for Part 1 (122 HV) and Part 2 (124 HV) are close to the theoretical value specified by the material datasheet (120 HV). The variation in the hardness measurements reported in Table 5 could be due to error in measurements due to the small sizes of the samples.

With regard to mass manufacturability, micro-moulding of polymers is already being implemented on an industrial scale, and micro-moulding of metals has the same potential. The moulding processes themselves are relatively short (tens of seconds), and the longest time was used to position the components manually into the inserts at each overmoulding stage. Automating the insert loading process would overcome this obstacle on a mass-manufacturing scale.

Figures 7 and 8 indicate the feasibility of the presented process chain in producing metallic movable joints with micro-scale interface by μPIM after addressing the main five challenges highlighted in the introduction. It should be noted, however, that the fabrication strategy has a number of limitations that need to be addressed. One limitation is that each stage of the process is effectively a micro-moulding process, which requires the geometry design to be demouldable from a two-half mould. This limits the producible geometries relative to, for example, SLS. In addition, all dimensions of the powder components are limited by the particle size, as it is recommended that the minimum feature size should be at least 10-20 times the particle size, as recommended by German (2009) and Piotter et al. (2005).

It should also be noted that the dimensional accuracy of the replicated components can be as good as the corresponding mould dimensions themselves. Although the designed distance between the moving components was 235 μm , the actual moulded POM layer was 246 μm at its narrowest point due

to machining variations. This resulted in a post-sintered cavity distance of 218 μm with an extra 9% increase in cavity size.

Future work will focus on overcoming such limitations by improved geometry design and process control. Research will also focus on implementing the process for smaller structure size and a variety of powder materials.

5. Conclusion

This paper presents a processing strategy for creating micro-scale cavities between moving components. The proposed process route combines the capabilities of powder micro-moulding, micro-overmoulding, catalytic debinding and sintering. An articulated structure with a single degree of freedom was used as a demonstrator for the technology. The produced components showed that the process routes are feasible and no serious challenges were encountered, except for the need to investigate other mould-fabrication methods and optimise process conditions for dimensional control. Density measurements showed that the components were approximately 84% of the theoretical density, which is due to sintering taking place below the recommended temperature. Hardness measurements showed average values close to the theoretical values. Further experimentation is required to assess the feasibility of the process for smaller, micro-scale dimensions and for different powder-based materials.

Acknowledgements

The authors would like to thank the EPSRC and the Cranfield IMRC for their support of this work.

References

- Abolhasani, H., Muhamad, N., 2010. A new starch-based binder for metal injection molding. J. Mater. Process. Tech., 210, 961–968.
- Attia, U. M., Alcock, J. R., 2011a. A review of micro-powder injection moulding as a microfabrication technique. J. Micromech. Microeng., 21, art. no. 043001.
- Attia, U. M., Alcock, J. R., 2011b. Fabrication of ceramic micro-scale hollow components by micro-powder injection moulding. J. Eur. Ceram. Soc., 32, 1199-1204

493 Attia, U. M., Alcock, J. R., 2012. Fabrication of hollow, 3D, micro-scale metallic structures by micro-
 494 powder injection moulding. J. Mater. Process. Tech., 212, 2148-2153.

495 Bloemacher, M., Weinand, D., 1997. Catamold - a new direction for powder injection molding. J. Mater.
 496 Process. Tech., 63, 918-922.

497 Castro, L., Merino, S., Levenfeld, B., Várez, A., Torralba, J.M., 2003. Mechanical properties and pitting
 498 corrosion behaviour of 316L stainless steel parts obtained by a modified metal injection moulding
 499 process. J. Mater. Process. Tech., 143–144, 397–402.

500 Fan, L., Tai, Y., Muller, R. S., 1988. Integrated movable micromechanical structures for sensors and
 501 actuators. IEEE T. Electron. Dev., 35, 724-730.

502 Field, J., 2008. Two to five year follow-up of the LPM ceramic coated proximal interphalangeal joint
 503 arthroplasty. J. Hand Surg.-Eur. Vol., 33, 38-44.

504 Fu, G., Loh, N. H., Tor, S. B., Murakoshi, Y., Maeda, R., 2004. Replication of metal microstructures by
 505 micro powder injection molding. Materials and Design, 25, 729–733.

506 Fu, G., Loh, N. H., Tor, S. B., Murakoshi, Y., Maeda, R., 2005a. Effects of injection molding parameters
 507 on the production of microstructures by micropowder injection molding. Mater. Manuf. Process.,
 508 20, 977–985.

509 Fu, G., Loh, N. H., Tor, S. B., Tay, B. Y., Murakoshi, Y., Maeda, R., 2005b. Injection molding,
 510 debinding and sintering of 316L stainless steel microstructures. Appl. Phys. A-Mater., 81,495–500.

511 German, R. M., 1998. A rationalization of the powder injection molding process for stainless steels based
 512 on component feature. International Conference and Exhibition on Powder Metallurgy and
 513 Particulate Materials, pp 5.71–5.83.

514 German, R. M., 2009. Medical and dental applications for microminiature powder injection moulding
 515 (microPIM) – a roadmap for growth. PIM International, 3, 21-29.

516 German, R. M. and Atre, S. V., 2013. Pro Forma Report of Trends and Forecasts for PIM. Online source
 517 at: <http://pim2013marketstudy.scipivision.com>. Accessed 2013.

518 Hassanin, H., Jiang, K., 2010. Optimized process for the fabrication of zirconia micro parts.
 519 Microelectron. Eng., 87, 1617-1619.

520 Hergert, R., Ku, I. S. Y., Reddyhoff, T., Holmes, A. S., 2010. Micro rotary ball bearing with integrated
 521 ball cage: fabrication and characterization. 23rd IEEE International Conference on Micro Electro
 522 Mechanical Systems, MEMS 2010, Hong Kong, pp. 687-690.

523 Huang, M-S., Hsu, H-C., 2009. Effect of backbone polymer on properties of 316L stainless steel MIM
 524 compact. J. Mater. Process. Tech., 209, 5527–5535.

525 Imgrund, Ph., Rota, A., Simchi, A., 2008. Microinjection moulding of 316L/17-4PH and 316L/Fe
 526 powders for fabrication of magnetic–nonmagnetic bimetals. J. Mater. Process. Tech., 200, 259-264.

527 Kim, K., Liu, X., Zhang, Y., Sun, Y., 2008. MicroNewton force-controlled manipulation of biomaterials
 528 using a monolithic MEMS microgripper with two-axis force feedback. 2008 IEEE International
 529 Conference on Robotics and Automation, ICRA 2008, Pasadena, CA. 3100-3105.

530 Koch, R., Sandoz, W., 1994. Finger joint Prosthesis made of metal. US Patent: 5,290,314.

531 Kong, X., Barriere, T., Gelin, J.C., 2012. Determination of critical and optimal powder loadings for 316L
 532 fine stainless steel feedstocks for micro-powder injection molding. J. Mater. Process. Tech., 212,
 533 2173– 2182.

534 Leong, T. G., Zarafshar, A. M., Gracias, D. H., 2010. Three-dimensional fabrication at small size scales.
 535 Small, 6, 792-806.

536 Li, S. G., Fu, G., Reading, I., Tor, S. B., Loh, N. H., Chaturvedi, P., Yoon, S. F., Youcef-Toumi, K., 2007.
 537 Dimensional variation in production of high-aspect-ratio micro-pillars array by micro powder
 538 injection molding. Appl. Phys. A-Mater., 89, 721–728.

539 Li, Y., Liu, S., Qu, X., Huang, B., 2003. Thermal debinding processing of 316L stainless steel powder
 540 injection molding compacts. J. Mater. Process. Tech., 137, 65–69.

541 Ling, Z., Lian, K., 2007. In situ fabrication of SU-8 movable parts by using PAG-diluted SU-8 as the
 542 sacrificial layer. Microsyst. Technol., 13, 253-257.

543 Liu, L., Loh, N. H., Tay, B. Y., Tor, S. B., Murakoshi, Y., Maeda, R., 2005. Mixing and characterisation
 544 of 316L stainless steel feedstock for micro powder injection molding. Mater. Charact., 54, 230–238.

545 Liu, L., Loh, N. H., Tay, B. Y., Tor, S. B., Murakoshi, Y., Maeda, R., 2007. Effects of thermal debinding
 546 on surface roughness in micro powder injection molding. Mater. Lett., 61, 809–812.

547 Loh, N. H., Tor, S. B., Tay, B. Y., Murakoshi, Y., Maeda, R., 2003. Micro powder injection molding of
 548 metal microstructures. Mater. Sci. Forum, 426–432, 4289–4294.

549 Manonukul, A., Muenya, N., Léaux, F., Amaranan, S., 2010. J. Mater. Process. Tech., 210, 529–535.

550 Middleton, A., Lakshmipathy, R., Irwin, L.R., 2011. Failures of the RM finger prosthesis joint
551 replacement system. J. Hand Surg.-Eur. Vol., 36E, 599-604.

552 Nishiyabu, K., Kanoko, Y., Tanaka, S., 2007. Innovations in micro metal injection molding process by
553 lost form technology. Mater. Sci. Forum, 534–536, 369–372.

554 Omar, M. A., Ibrahim, R., Sidik, M. I., Mustapha, M., Mohamad, M., 2003. Rapid debinding of 316L
555 stainless steel injection moulded component. J. Mater. Process. Tech., 140, 397-400.

556 Piotter, V., Finnah, G., Oerlygsson, G., Ruprecht, R., Haußelt, J., 2005. Special variants and simulation of
557 micro injection moulding. Injection Moulding 2005: Collected Papers of the 5th International
558 Conference, Copenhagen, Denmark, 1–2 March 2005.

559 Piotter, V., Hanemann, T., Heldele, R., Mueller, M., Mueller, T., Plewa, K., et al., 2010a. Metal and
560 ceramic parts fabricated by microminiature powder injection molding. Int. J. Powder Metall., 46, 21-
561 28.

562 Piotter, V., Mueller, T., Plewa, K., Ritzhaupt-Kleissl, H.-J., Ruh, A., Hausselt, J., 2010b. One- and two-
563 component micro powder injection moulding derived from thermoplastic microreplication. Plast.
564 Rubber Compos., 39, 287-292.

565 Pister, K. S. J., Judy, M. W., Burgett, S. R., Fearing, R. S., 1992. Microfabricated hinges. Sensor Actuat.
566 A-Phys., 33, 249-256.

567 Rafi Raza, M., Ahmad, F., Omar, M. A., German, R. M., 2012. Effects of cooling rate on mechanical
568 properties and corrosion resistance of vacuum sintered powder injection molded 316L stainless steel.
569 J. Mater. Process. Tech., 212, 164– 170.

570 Rota, A., 2002. New features in material issues for metallic micro components by MIM. Proc. PM2TEC
571 pp 10/49–/57

572 Ruh, A., Dieckmann, A.-M., Heldele, R., Piotter, V., Ruprecht, R., Munzinger, C., et al. (2008).
573 Production of two-material micro-assemblies by two-component powder injection molding and
574 sinter-joining. Microsyst. Technol., 14, 1805-1811.

575 Ruh, A., Piotter, V., Plewa, K., Ritzhaupt-Kleissl, H.-J., Haußelt, J., 2010. Effects of material
576 improvement and injection moulding tool design on the movability of sintered two-component
577 micro parts. Microsyst. Technol., 16, 1989-1994.

578 Samanta, S. K., Chattopadhyay, H., Godkhindi, M. M., 2011. Thermo-physical characterization of binder
 579 and feedstock for single and multiphase flow of PIM 316L feedstock. J. Mater. Process. Tech., 211,
 580 2114– 2122.

581 Seidemann, V., Rabe, J., Feldmann, M., Büttgenbach, S., 2002. SU8-micromechanical structures with in
 582 situ fabricated movable parts. Microsyst. Technol., 8, 348-350.

583 Tay, B. Y., Liu, L., Loh, N. H., Tor, S. B., Murakoshi, Y., Maeda, R., 2005. Surface roughness of
 584 microstructured component fabricated by μ MIM. Mat. Sci. Eng. A-Struct., 396, 311–319.

585 Waits, C. M., Geil, B., Ghodssi, R., 2007. Encapsulated ball bearings for rotary micro machines. J.
 586 Micromech. Microeng., 17, S224-S229.

587 Yang, Y., Su, X., Wang, D., Chen, Y., 2011. Rapid fabrication of metallic mechanism joints by selective
 588 laser melting. P. I. Mech. Eng. B-J. Eng., 225, 2249-2256.

589 Zhu, Z., Hassanin, H., Jiang, K., 2010. A soft moulding process for manufacture of net-shape ceramic
 590 microcomponents. Int. J. Adv. Manuf. Tech., 47, 147-152.

2013-09-09

Creating movable interfaces by micro-powder injection moulding

Attia, Usama M.

Elsevier

U.M. Attia, M. Hauata, I. Walton, D. Annicchiarico, J.R. Alcock, Creating movable interfaces by micro-powder injection moulding, Journal of Materials Processing Technology, Volume 214, Issue 2, February 2014, Pages 295-303

<http://dx.doi.org/10.1016/j.jmatprotec.2013.09.012>.

Downloaded from Cranfield Library Services E-Repository